Mapping carotenoid content in vineyards using high-resolution hyperspectral imagery acquired from an unmanned aerial vehicle

P.J. Zarco-Tejada[1], M.L. Guillén-Climent[1], R. Hernández-Clemente[2], A. Catalina[3], M.R. González[3], P. Martín[3]

[1]Instituto de Agricultura Sostenible (IAS), Consejo Superior de Investigaciones Científicas (CSIC), Córdoba, Spain

[2] ETSIAM, Dpto. de Ingeniería Forestal, Universidad de Córdoba, Córdoba, Spain

[3] Departamento de Producción Vegetal y Recursos Forestales, ETS de Ingenierías Agrarias, Universidad de Valladolid, Palencia, Spain

Corresponding author:

Pablo J. Zarco-Tejada
Instituto de Agricultura Sostenible (IAS)
Consejo Superior de Investigaciones Científicas (CSIC)
Alameda del Obispo, s/n
14004 - Córdoba
Spain
Tel: +(34) 957 499 280; +(34) 676 954 937
Fax: +(34) 957 499 252
e-mail: pzarco@ias.csic.es
http://quantalab.ias.csic.es

Submitted to *Agricultural and Forest Meteorology o IEEE-TGRS*
January 2012

Abstract

Chlorophyll a+b (C_{a+b}), carotenoids (C_{x+c}) and anthocyanins (Anth) are photosynthetic pigments associated with photosynthesis, participation in light harvesting and energy transfer, quenching and photoprotection. This manuscript makes progress on developing methods for carotenoid content estimation in vineyards using high resolution hyperspectral imagery acquired from an unmanned aerial vehicle (UAV). Imagery was acquired over three years using two different UAV platforms, a 6-band multispectral camera and a micro-hyperspectral imager flown in the spectral mode of 260 bands at 1.85 nm/pixel at 12-bit radiometric resolution, yielding 40 cm resolution and a FWHM of 6.4 nm with a 25-micron slit in the 400-885 nm spectral region. Field data collections were conducted in August 2009, 2010 and 2011 in the western area of Ribera del Duero *Appellation d'Origine,* northern Spain. A total of twelve full production vineyards and two study plots per field were selected to assure appropriate variability in leaf biochemistry and vine physiological conditions. Leaves were collected for destructive sampling and biochemical determination of chlorophyll *a*+*b* and carotenoids conducted in the laboratory. In addition to leaf sampling and biochemical determination, canopy structural parameters were measured on each 10 m x 10 m plot, such as grid size, number of vines within each plot, trunk height, plant height and width, and row orientation. The R_{515}/R_{570} index recently proposed for carotenoid estimation in conifer forest canopies was investigated in this study for the case of vineyards. The leaf radiative transfer model PROSPECT-5 which simulates the carotenoid and chlorophyll content effects on leaf reflectance and transmittance was linked with canopy-level radiative transfer models SAILH and FLIGHT, as well as to simpler approximations based on infinite reflectance R_∞ formulations. The objective was to simulate the pure vine reflectance without soil and shadow effects due to the high resolution hyperspectral imagery acquired which enabled targeting pure vines. The model simulation results with synthetic spectra demonstrated the effects due to C_{a+b} content on the C_{x+c} retrieval when the R_{515}/R_{570} index is used. Therefore, *scaling up* methods were proposed for carotenoid content estimation based on the combined R_{515}/R_{570} (sensitive to C_{x+c}) and TCARI/OSAVI (sensitive to C_{a+b}) narrow-band indices. Results demonstrated the feasibility for mapping carotenoid concentration at the pure vine level, yielding RMSE values below 1.3 μg/cm^2 for the two years investigated with hyperspectral imagery using SAILH and FLIGHT models. The infinite reflectance model by Yamada and Fujimura yielded the best results, obtaining RMSE values below 0.95 μg/cm^2 consistently for the two years investigated with the micro-hyperspectral imager. These results demonstrate that a simpler modelling approximation may be valid when high resolution imagery is used that enables targeting pure vines without shadow and background effects.

Keywords: hyperspectral, airborne, carotenoid, chlorophyll, R_{515}/R_{570}, TCARI/OSAVI, vineyards, UAV, scaling up

1. Introduction

Leaf biochemical constituents, such as chlorophyll a+b (C_{a+b}), water (C_w), dry matter (C_m) are physiological indicators used as a proxy of stress that may be estimated by remote sensing data in the 400-2500 nm spectral region. In particular, several studies demonstrate that estimating chlorophyll content in leaves is feasible using leaf reflectance and transmittance (Jacquemoud *et al*, 1996; Carter and Spiering, 2002; Sims and Gamon, 2002; Gitelson *et al*., 2003; le Maire *et al*., 2004). For this purpose, large number of narrow-band indices calculated from hyperspectral reflectance have been tested with success in different crops (Haboudane *et al.,* 2002; 2004; Zarco-Tejada *et al.*, 2001; a full review of indices can be found in Zarco-Tejada *et al.*, 2005). Recently, combined indices sensitive to C_{a+b} content have been developed with the *Transformed Chlorophyll Absorption in Reflectance Index,* TCARI (Haboudane *et al*., 2002), and the *Optimized Soil-Adjusted Vegetation Index,* OSAVI (Rondeaux *et al.,* 1996), used to minimize soil and LAI effects in closed crops (Haboudane *et al*., 2002), tree orchards (Zarco-Tejada *et al*., 2004) and vineyards (Zarco-Tejada et al., 2005; Martin et al., 2007; Meggio et al., 2010).

Carotenoids (C_{x+c}) are also important photosynthetic pigments, which include two carotenes and five xanthophylls (Demmig-Adams & Adams, 1992). Carotenoids are physiologically important because of its role associated with photosynthesis, participation in light harvesting and energy transfer (Frank & Cogdell, 1996; Ritz et al., 2000), quenching and photoprotection (Thayer & Björkman 1990, Young & Britton 1990; Demmig-Adams, 1998). Nevertheless, less efforts on carotenoid content have been conducted due to the difficulties associated with the overlapping absorption in the blue /

green region caused by photosynthetic pigments such as C_{a+b}, C_{x+c} and anthocyanins (Anth). The overlapping absorption by chlorophyll and carotenoids in the 400-700 nm region poses a problem when trying to retrieve both C_{a+b} and C_{x+c} concentration independently (Feret et al., 2011). In addition, some indices have been identified sensitive to C_{x+c}, but they generally work well at the leaf level with high effects caused by the canopy structure (Meggio et al., 2010; Hernández-Clemente et al., 2011). In addition, the progress made on carotenoid content estimation has became even more difficult in vineyards because they are complex heterogeneous canopies with large effects caused by shadows and soil components as a function of the sun angle and row orientation (Ref., Guillén-Climent (in revision)??).

The main spectral bands proposed for C_{x+c} estimation in the visible/NIR region are based on band ratios in the 700 nm region (678, 708 and 760 nm) and the green region (500, 550 nm) (Chappelle et al., 1992; Merzlyak et al., 1999). Also, some indices have been proposed using the 800 nm band combined with 470, 680, and 635 nm bands (Peñuelas et al., 1995; Blackburn 1998). In particular, the work conducted by Chappelle et al. (1992) concluded that C_{x+c} showed fraction a maximum absorption peak at 500 nm, proposing ratios such as R_{760}/R_{500} for C_{x+c} estimation. Other authors (Gamon et al., 1992; Gitelson et al., 2003, 2006; Garrity et al., 2011; Hernández-Clemente et al., 2011) proposed using visible ratios, and specific leaf-level studies conducted by Gitelson et al. (2002) showed that C_{x+c} absorption was directly related to a spectral absorption at 520 nm. They proposed the *Carotenoid Concentration Index* as $(1/R_{515})-(1/R_{550})$ and $(1/R_{515})-(1/R_{700})$ (Gitelson et al., 2002).

Nevertheless, these studies rely entirely on leaf level work and require the scaling up to the canopy level, assessing the effects caused on the proposed indices by the structure and background due to mixed pixels. In particular, the validity of leaf-level indices for pigment content estimation in vineyards from airborne imagery were studied through the linked PROSPECT (Jaquemoud and Baret, 1990) and rowMCRM models. Through this approach, the effects of vineyard structure, vine dimensions, row orientation and soil and shadow effects on the canopy reflectance could be assessed for the case of C_{a+b} estimation (Zarco-Tejada et al., 2005). Using this methodology, relationships for C_{a+b} content with TCARI/OSAVI enabled mapping chlorophyll content in 24 vineyards using CASI airborne imagery, yielding r^2=0.67 and RMSE=11.5 μg/cm^2.

Nevertheless, these methods that require accounting for the row structure and orientation, soil effects and canopy LAI variation may be critical in the case of vineyards when using image resolutions in the range 1 – 2 m pixel size. The pure vine reflectance cannot be extracted without soil and shadow contributions at spatial resolutions greater than 1 m. Simpler canopy-level approximations without the need for considering the structure may work well when higher spatial resolution is used (below 50 cm pixel size in the case of vineyards) because the extraction of the pure vine reflectance removing shadow and soil background effects is then feasible. Under these assumptions of targeting pure dense vines, infinite reflectance formulations may be proposed as a simpler approximation as they model the reflectance without canopy structure or viewing geometry considerations, based solely on leaf reflectance and transmittance (see Zarco-Tejada et al., 2001). These formulations are valid for optically-thick leaf material with different assumptions for the multiple scattering. Lillestaeter (1982), Miller et al. (1992), Yamada and Fujimura, (1991) and Hapke (1993) discussed these infinite reflectance models, applied with success to forest sites for C_{a+b} estimation (Zarco-Tejada et al., 2001) and for equivalent water thickness estimation (Riaño et al., 2005).

Nevertheless, more complex approaches can also be used to model the pure vine reflectance in the case of high resolution which enables the removal of mixed pixels and shadow effects. Under these conditions, approximations based on turbid-medium assumptions (such as in the case of SAILH) when targeting pure canopy pixels (Zarco-Tejada et al., 2001) and more computational expensive approximations such as in the case of the Forest Light Interaction Model (FLIGHT) may be more appropriate. In particular, the 3-D model FLIGHT is based on Monte Carlo ray tracing method to simulate the radiative transfer in a canopy structure (North, 1996) and was previously used to simulate row-structured canopy reflectance in olive orchards (Suárez et al., 2008), peach and orange orchards (Guillén-Climent et al., in press) and more recently simulating row-structured vineyards for fIPAR estimation (Guillén-Climent et al., submitted).

Therefore, the assessment of a C_{x+c} sensitive index linked with different scaling up approaches is the main focus of this manuscript. Recently, the index R_{515}/R_{570} was proposed by Hernandez-Clemente for forestry sites, demonstrating to be significantly related with C_{x+c} concentration both at leaf ($r^2>0.72$; $P<0.001$) and canopy levels ($r^2>0.71$; $P<0.001$). In such study, coefficients of determination between C_{x+c} concentration and other published narrow-band indices sensitive to C_{x+c} revealed that were highly related with C_{x+c} content at leaf level but highly affected by structural parameters at crown level.

Nevertheless, the effects of C_{a+b} content on this proposed R_{515}/R_{570} index have not been assessed yet. This manuscript proposes the estimation of both C_{x+c} and C_{a+b} using R_{515}/R_{570} and TCARI/OSAVI simultaneously through a scaling up approach based on different canopy reflectance simulations.

2. Materials and Methods

2.1. Field experiments and airborne campaigns

2.1.1. Field data collection

Field data collections were conducted in August 2009, 2010 and 2011 in the western area of Ribera del Duero *Appellation d'Origine* (northern Spain). A total of 12 full production vineyards belonging to a plot network currently monitored by the local government were selected to assure appropriate variability in leaf biochemistry and vine physiological conditions. All vineyards consisted on cv. Tempranillo grafted on 110-Richter rootstock, with ages ranging between 7 and 16 years. The soils are calcareous, poor in organic matter, with a medium-weighed texture and an average pH of 8.7. Concentrations of active carbonate (up to 17.6%) and DPTA extractable Fe (1.2 to 7.6 $mg \cdot kg^{-1}$) are highly heterogeneous within the study areas. The field data collection was conducted on 24 sub-areas of 10 m x 10 m located in each of the 12 selected vineyards. Vine density ranged between 2200 and 4000 vines per hectare, and plants were trained to a simple or double Cordon Royat system (as described in detail in Martín *et al.,* 2007). The vineyards under study ranged in physiological status, canopy structure, soil background, and planting row orientation.

The leaves used for destructive sampling and biochemical determination were sampled from the top of the canopy, eliminating the small leaves indicative of low expansion. Leaves were placed in paper bags and then stored in a freezer at -8°C prior to pigment determination. A 1.6 cm circle from each leaf sample was cut out for grinding with 4 ml acetone at 80%, and adding 8 ml acetone to a total of 12 ml in each tube. Tubes were stored in the dark at 4°C for 48 hours prior to spectrophotometer measurements. Each sample for pigment determination was filtered, placed in a cuvette and the absorbance measured between 400 nm and 700 nm with 2 nm fixed resolution at 1 nm interval with a Jasco V-530 UV-VIS spectrophotometer (Jasco Inc., Great Dunmow, UK). Chlorophyll *a* (C_a), chlorophyll *b* (C_b), and total carotenoid (C_{x+c}) concentration were calculated using the extinction coefficients derived by Wellburn (1994) and the absorbance measured at 470 nm, 646 nm, and 663 nm with Equations [1]-[3].

$$C_a = 12.21 \cdot A_{663} - 2.81 \cdot A_{646} \quad [1]$$

$$C_b = 20.13 \cdot A_{646} - 5.03 \cdot A_{663} \quad [2]$$

$$C_{x+c} = (1000 \cdot A_{470} - 3.27 \cdot C_a - 104 \cdot C_b) / 198 \quad [3]$$

A subset of leaves was used to measure bands R_{515}, R_{530} and R_{570} with a customized PlantPen instrument (Photon Systems Instruments, Brno, Czech Republic). The same leaves were used to measure leaf C_{a+b} and C_{x+c} to derive relationships between the R_{515}/R_{570} and the biochemical measurements.

In addition to leaf sampling and biochemical determination, canopy structural parameters were conducted on each 10 m x 10 m plot, such as grid size, number of vines within each plot, trunk height, plant height and width, and row orientation. The leaf area index (LAI) and sunlit canopy cover in each study area were estimated using allometric methods. Yield and vigor (pruning weight) of the vines were also determined at each study site. A summary of the structural data measured to characterize each study area is described in Table 1.

2.1.2. Airborne campaigns

Airborne campaigns were conducted in 2009 with a narrow-band multispectral camera, and in 2010 and 2011 using a micro-hyperspectral imager. Flights were conducted using two different unmanned aerial vehicles (UAVs) operated by the *Laboratory for Research Methods in Quantitative Remote Sensing* (QuantaLab, IAS-CSIC, Spain) (Berni *et al.,* 2009b; Zarco-Tejada *et al*., 2008; 2012).

An *unmanned aerial vehicle* (UAV) platforms used for remote sensing research were developed to carry payloads with thermal, multispectral and hyperspectral imaging sensors. The two UAV platforms operated in this experiment consisted of a 2-m fixed-wing platform capable of carrying a 3.5 kg payload for 1 hour endurance at 5.8 kg take-off weight (TOW) (mX-SIGHT, UAV Services and Systems, Germany). This platform was used to fly the multispectral camera flown over the study sites in 2009, as well as to carry a thermal camera used for water stress detection part of other studies (Gonzalez-Dugo et al., 2012). A second UAV platform was developed for hyperspectral imagery acquisition, consisting on a 5-m wingspan fixed-wing platform capable of carrying a 3 kg payload for

1.5 hour endurance at 13.5 kg take-off weight (TOW) (Viewer, ELIMCO, Seville, Spain). This larger platform enabled the acquisition of carrying both the micro-hyperspectral imager and the thermal camera concurrently.

Both UAV platforms were controlled by an autopilot for autonomous flight (AP04, UAV Navigation, Madrid, Spain) to follow a flight plan using waypoints. The autopilot comprises a dual CPU controlling an integrated *Attitude Heading Reference System* (AHRS) based on a L1 GPS board, 3-axis accelerometers, gyros and a 3-axis magnetometer (Berni *et al*., 2009b). The ground control station and the UAV were radio linked transmitting position, attitude and status data at 20 Hz frequency; this tunneling transmission link also acted for communication purposes for the operation of remote sensing hyperspectral and multispectral cameras on board the UAVs.

The multispectral sensor flown in 2009 was a 6-band multispectral camera consisting of 6 independent image sensors and optics with user-configurable 10 nm full-width at half maximum (FWHM) spectral filters (Berni *et al.,* 2009; Zarco-Tejada *et al.,* 2009). The image resolution is 2592 x 1944 pixels with 10 bit radiometric resolution, optics focal length of 8.4 mm, and angular field of view (FOV) of 38.04º x 28.53º, yielding 15 cm spatial resolution at 150 m flight altitude. The bandsets selected for this study comprised centre wavelengths located at 515, 530, 570, 670, 700 and 800 nm. The multispectral images acquired over each vineyard field enabled the identification of the study areas used for the leaf sampling and ground structural measurements. The 2009 airborne campaign was conducted at 9.00 am GMT.

The hyperspectral imager installed on board the UAV was a micro-hyperspectral camera (Micro-Hyperspec VNIR model, Headwall Photonics, MA, USA) flown in the spectral mode of 260 bands at 1.85 nm/pixel at 12-bit radiometric resolution, yielding a FWHM of 3.2 nm with a 12-micron slit, and 6.4 nm with a 25-micron slit in the 400-885 nm region. Data acquisition and storage on board the UAV was set to 50 fps, and integration time was 18 ms. The 8-mm optics focal length yielded an IFOV of 0.93 mrad, an angular FOV of 50º, obtaining a swath of 522 m at 53x42 cm resolution, resampled to 40 cm for a flight conducted at 575 m AGL altitude and 75 km/h ground speed. The airborne campaigns over the vineyard fields consisted on flightlines acquired in the solar plane at 9.00 am GMT on August 2010 and 2011, using the CropSight UAV platform on 2010, and the Viewer UAV platform on 2011. For identification purposes, each plot was marked in the field using ground control points detectable in the imagery.

The multispectral and hyperspectral sensors were radiometrically calibrated using coefficients derived in the laboratory using a calibrated uniform light source (integrating sphere, CSTM-USS-2000C Uniform Source System, LabSphere, NH, USA) at four different levels of illumination and six integration times. The atmospheric correction was conducted using the total incoming irradiance at 1 nm intervals simulated with the SMARTS model developed by the National Renewable Energy Laboratory, US Department of Energy (Gueymard, 1995; 2001) using aerosol optical depth measured at 550 nm with a Micro-Tops II sunphotometer (Solar LIGHT Co., Philadelphia, PA, USA). Sunphotometer measurements were acquired at the time of the flights. The SMARTS model computation for clear sky spectral irradiance was validated to match the output from the MODTRAN complex band models within 2%, but using aerosol optical depth as input. This radiative transfer model has been previously used in other studies to perform the atmospheric correction of narrow-band multispectral imagery, such as in Berni *et al*. (2009b) and Suárez *et al.* (2010), and the atmospheric correction of the micro-hyperspectral imagery on board an UAV platform for chlorophyll fluorescence detection (Zarco-Tejada et al., 2012).

Ortho-rectification of the hyperspectral imagery acquired with the UAV platforms was conducted using PARGE (ReSe Applications Schläpfer, Wil, Switzerland) from data acquired with an inertial measuring unit (IMU) installed on board and synchronized with the hyperspectral imager. The hyperspectral imagery (Figure 1a;b) acquired enabled pure vine identification for field validation purposes, successfully separating pure vine from shaded and sunlit soil reflectance in most cases (Figure 1c), obtaining pure vine reflectance, sunlit and shaded soil components separately (Figure 1d). Each single pure vine from each vineyard field was identified using automatic object-based crown-detection algorithms. This method enabled the extraction of the mean radiance and reflectance for the 260 spectral bands acquired for vegetation index calculation from vines identified from each chlorotic and healthy study site (Figure 2).

2.2. Modeling the retrieval of carotenoid content with the R_{515}/R_{570} index

The R_{515}/R_{570} index proposed for carotenoid estimation in conifer forest canopies (Hernandez-Clemente et al., submitted) was investigated in this study for the case of vineyard row-structured canopies. The leaf radiative transfer model PROSPECT-5 (Jacquemoud & Baret, 1990; Féret et al., 2008) which simulates the carotenoid and chlorophyll content effects on leaf reflectance and transmittance was linked with canopy-level radiative transfer models as well as to simpler approximations based on infinite reflectance (R_∞) formulations. The very high resolution imagery used in this study between years 2009 and 2011 (15 cm resolution in the case of the multispectral imagery, 40 cm in the case of the hyperspectral imagery) and the pure-vine identification methods conducted from the imagery which avoided shadows and soil pixels allowed the assessment of different canopy-level approximations. The retrieval capability of the carotenoid content on pure vines through the R_{515}/R_{570} index was then assessed.

The PROSPECT-5 model was used to simulate leaf reflectance and transmittance for varying chlorophyll C_{a+b} (30-80 μg/cm^2) and carotenoid content C_{x+c} (4-14 μg/cm^2). The simulated leaf reflectance and transmittance spectra were used to calculate the R_{515}/R_{570} index, observing the effects caused by C_{a+b} and C_{x+c}. Figure 3 shows the effects of C_{a+b} and C_{x+c} on the leaf reflectance for the 400-600 nm spectral region where the R_{515}/R_{570} index is calculated.

Different approaches were used to simulate the pure vine reflectance from leaf-level reflectance and transmittance spectra: i) using simpler formulations based on infinite reflectance R_∞ simulations; and ii) using canopy reflectance radiative transfer models. The different levels of complexity used for simulating the pure vine reflectance was justified due to the retrieval methodology conducted for extracting the pure vegetation pixels from the imagery, which removed or at least diminished the structure due to the very high spatial resolution used.

The infinite reflectance R_∞ formulations simulate the reflectance without canopy structure or viewing geometry considerations, based solely on leaf reflectance and transmittance. These R_∞ formulations simulate optically-thick leaf material, assuming different multiple scattering approaches between leaf layers. This leaf-stack concept may have applicability to simulate a dense vine planted in wall-structured architectures, with little effect caused by the soil background and shadows. Nevertheless, it cannot take into consideration the viewing angle effects or the row orientation for each vineyard field under study. Comparison of the performance of these R_∞ formulations against canopy reflectance models was conducted in Zarco-Tejada et al. (2001). Different R_∞ formulations have been derived based on assumptions related to the scattering between layered leaves, expressing the optically thick medium in terms of the single leaf reflectance and transmittance. Lillestaeter (1982) ($R_{\infty 1}$) [Equation 4a], Yamada and Fujimura (1991) ($R_{\infty 2}$) [Equation 4b] and Hapke (1993) ($R_{\infty 3}$) [Equation 4c] formulations were calculated from simulated leaf reflectance and transmittance using PROSPECT-5. The spectra was then used to calculate the canopy-level R_{515}/R_{570} index as a function of the varying leaf inputs indicated above.

$$R_{\infty 1} = \frac{\rho}{1-\tau^2} \qquad [4a]$$

$$R_{\infty 2} = \frac{\rho}{1-\dfrac{2\tau^2}{1+(1-4\tau^2)^{1/2}}} \qquad [4b]$$

$$R_{\infty 3} = \frac{1-\alpha^{1/2}}{1+\alpha^{1/2}}; \quad \alpha = 1-\rho-\tau \qquad [4c]$$

Regarding the canopy models used, a simpler radiative transfer approach was conducted with the *Scattering by Arbitrary Inclined Leaves* (SAIL) (Verhoef, 1984) adapted to take into account the hotspot effect or the multiple scattering in the canopy (SAILH) (Kuusk, 1985). The SAILH model approximates the canopy as a horizontally uniform parallel-plane infinitely-extended medium, with diffusely reflecting and transmitting elements. Although the vine canopy reflectance cannot be considered as a plane-parallel canopy, the use of SAILH was justified in this study for two reasons: i) ease of operation and calculations when linked to PROSPECT-5, which enabled the generation of synthetic spectra with low computational effort. These databases are generated in this study to assess the retrieval performance of R_{515}/R_{570} for carotenoid determination under different assumptions, including LAI variation; ii) the methodology conducted aimed at estimating carotenoid content from pure vine reflectance extracted after removing any shadow and soil pixel effects. Therefore the use of SAILH model may be valid for these high-resolution pure-vine retrieval conditions. SAILH inputs are: canopy architecture defined by the leaf area index (LAI) and the leaf angle distribution function (LADF), leaf reflectance and transmittance, underlying soil reflectance, and the illumination and viewing geometry (solar zenith and sensor viewing angles).

A more complex and computationally expensive approach used in this study consisted on simulating the vineyard scenes using the Monte-Carlo ray tracing 3-D Forest Light Interaction Model (FLIGHT) (North, 1996). The FLIGHT model has been previously used to simulate row-structured canopy reflectance in olive orchards for modelling the PRI index for stress detection (Suárez et al., 2008), and peach, orange and vineyard canopies for mapping and modelling the radiation interception (Guillén-Climent et al., submitted). In this work, the FLIGHT model was used to simulate the pure vine reflectance, extracting from the vineyard canopy simulation the reflectance from the centre of each vine row. The 3D vineyard scene was conducted using structural inputs within the range of variation of the field data measured for each field. Input parameters defining geometrical and optical properties for the different models can be found in Table 2, showing the multispectral imagery acquired for two orientations (Figures 4a and 4b), the FLIGHT scene generation obtained for each vineyard field (Figures 4c and 4d), showing the aggregated and pure vine reflectance extracted from the centre of the row (Figures 4e and 4f).

The effects of the leaf inputs C_{a+b}, C_{x+c}, and N, and the canopy parameters vine LAI, and soil reflectance were assessed within the range of variation for vineyard canopies (see Zarco-Tejada et al., 2005). Leaf inputs C_{a+b} (30-80 μg/cm^2), C_{x+c} (4-14 μg/cm^2), N (1.6-1.8) and canopy inputs LAI (1-3) and soil reflectance were ranged to calculate the index R_{515}/R_{570} proposed.

Scaling up relationships linking PROSPECT-5 and the different approximations proposed for simulating the vine reflectance were conducted: i) the three infinite reflectance R_∞ formulations ($R_{\infty1}$, $R_{\infty2}$, $R_{\infty3}$); ii) SAILH; and iii) FLIGHT. A synthetic spectra database was generated using 1000 random inputs for C_{a+b} and C_{x+c} for the ranges indicated, C_m (0-0.03), N (1.6-1.8), LAI (1-3), and soil reflectance variation. The database was used to develop each relationship (500 samples), using the remaining 500 samples to calculate the coefficient of determination and the RMSE for each scaling-up approach developed using R_∞, SAILH and FLIGHT canopy reflectance simulation approaches.

3. Results

3.1. Modeling results

Modelling results conducted with PROSPECT-5 linked to SAILH demonstrated a relationships between R_{515}/R_{570} and C_{x+c} as a function of C_{a+b} (Figure 5a), with little effects caused by the leaf N parameter (Figure 5b), LAI (Figure 5c) and insensitive to soil reflectance variation (Figure 5d). The simulations demonstrated that a family of relationships exists as a function of chlorophyll concentration, therefore being important to account for C_{a+b} when estimating C_{x+c}. Simulation results suggested that a same R_{515}/R_{570} index value (R_{515}/R_{570}=0.7) could be related to C_{x+c} ranging between 6 and 15 μg/cm^2 when C_{a+b} is set to 30 μg/cm^2 or 60 μg/cm^2 (Figure 5a).

The simulation study conducted with PROSPECT-5 and the different canopy approximations through infinite reflectance R_∞ formulations and SAILH is summarized in Table 3. The synthetic spectra database generated using 1000 random inputs for C_{a+b}, C_{x+c}, N, LAI, soil reflectance and C_m yielded different coefficients of determination and RMSE values as a function of different cases studied and simulation model used. Cases 1 to 4 tested (see Table 3 for the inputs fixed and varied in the modelling study) consisted on estimating C_{x+c} using models based on R_{515}/R_{570} only, while Case 5 included both R_{515}/R_{570}

(sensitive to C_{x+c}) and TCARI/OSAVI (sensitive to C_{a+b}). Cases 1 and 2 were built with known C_{a+b}, while Cases 3 and 4 allowed C_{a+b} to vary randomly. Cases 4 and 5 allowed the variation of all inputs; the only difference between Case 4 and Case 5 is that the latter used both R_{515}/R_{570} and TCARI/OSAVI to estimate C_{x+c} while Case 4 used only R_{515}/R_{570}.

As a results of the different modelling cases considered, the simulations conducted demonstrated that lower coefficients of determination and higher RMSE values were obtained when C_{a+b} was randomly varied and only R_{515}/R_{570} was used to estimate C_{x+c} (r^2=0.51; RMSE=1.99 μg/cm^2 for PROSPECT+SAILH). Nevertheless, when all parameters were allowed to vary randomly but C_{x+c} was estimated using both R_{515}/R_{570} and TCARI/OSAVI, the coefficients of determination and RMSE decreased largely (r^2=0.93; RMSE=0.73 for PROSPECT+SAILH). These simulation results using synthetic spectra confirm that estimating C_{x+c} with both R_{515}/R_{570} and TCARI/OSAVI yielded the best results due to the combined contribution of R_{515}/R_{570} (sensitive to C_{x+c}) and TCARI/OSAVI (sensitive to C_{a+b}).

Among the different canopy simulations proposed, the results obtained with the synthetic spectra database showed superior results for $R_{\infty 1}$ and $R_{\infty 3}$ among the infinite reflectance formulations. Results obtained with infinite reflectance models in the modelling study were similar to the SAILH model. These results obtained with infinite reflectance models, which are simpler approximations with no canopy structure consideration, suggest their validity when targeting pure pixels if structural effects are not critical. This may be the case when targeting pure vines if high resolution is used, as in this study. Next section shows the results obtained for C_{x+c} estimation when this methodology based on R_{515}/R_{570} and TCARI/OSAVI are applied to imagery acquired on 2009, 2010 and 2011 years using infinite reflectance formulations, SAILH, and the 3D monte-carlo FLIGHT model.

3.2. Experimental results

The leaf level measurements conducted with the PlantPen instrument (Photon Systems Instruments, Brno, Czech Republic) customized for carotene estimation with bands R_{515} and R_{570} bands showed a good relationship (r^2=0.84) between the R_{515}/R_{570} index and leaf C_{x+c} measured by destructive sampling (Figure 6). This result obtained at the leaf level confirms the previous modelling conclusions which demonstrated the sensitivity of the R_{515}/R_{570} index to C_{x+c} content.

The relationship between the R_{515}/R_{570} and C_{x+c} calculated from the airborne imagery for the three years under study (Figure 7) demonstrated consistent results, yielding r^2 values in the range 0.43 – 0.48, being statistically significant ($p<0.01$ for the three years). TCARI/OSAVI was also related to C_{a+b} with similar results (r^2=0.45; $p<0.01$; year 2010) (Figure 8) obtaining consistent results with previous studies published which assessed the sensitivity of TCARI/OSAVI to C_{a+b} in vineyards (Zarco-Tejada *et al.*, 2005). The relationship between TCARI/OSAVI and C_{a+b} was significant for 2009 (r^2=0.66; $p<0.001$) and 2010 (r^2=0.45; $p<0.01$), although no significant results were found for the year 2011 (r^2=0.1).

The methodology described earlier to estimate C_{x+c} was applied in the form C_{x+c} = f(R_{515}/R_{570}; TCARI/OSAVI) through scaling up simulations conducted PROSPECT-5 linked with the three infinite reflectance formulations ($R_{\infty1}$; $R_{\infty2}$; $R_{\infty3}$), SAIL and FLIGHT (Table 4). The best results among the three years were found for $R_{\infty2}$ (r^2=0.41-0.64), SAILH (r^2=0.2-0.56) and FLIGHT (r^2=0.26-0.58). The lowest RMSE errors were obtained for $R_{\infty2}$ model (RMSE=0.8-1.6 μg/cm^2), while FLIGHT performed better (RMSE=1.25-2.91 μg/cm^2) than SAILH (RMSE=1.08-4.6 μg/cm^2). Most of the errors were obtained in the imagery acquired in 2009 (multispectral imagery), while the 2010 and 2011 hyperspectral imagery yielded lower RMSE values (RMSE<1 μg/cm^2 for $R_{\infty2}$; RMSE<1.3 μg/cm^2 for SAILH and FLIGHT models).

The results obtained for estimating C_{x+c} from the hyperspectral imagery showed larger errors when using the $R_{\infty1}$ formulation (RMSE=3.23 μg/cm^2) as compared to $R_{\infty2}$ (RMSE=0.87 μg/cm^2) (Figure 9a). The comparison for SAILH and FLIGHT (Figure 9b) showed similar results among the two models used (RMSE<1.3 μg/cm^2 for both models). This methodology was applied at the vine level to two sample vineyard fields, estimating C_{x+c} using both R_{515}/R_{570} and TCARI/OSAVI indices acquired from the hyperspectral imager on board the unmanned aerial vehicle (Figure 10). The hyperspectral imagery acquired (Figure 10a; c) enabled the estimation of C_{x+c} (Figure 10b; d) assessing the within field spatial variability of carotenoid content at the vineyard level.

4. Conclusions

Modelling and experimental results obtained in this study demonstrated that estimating carotenoid content in vineyards using hyperspectral imagery was feasible yielding errors below 1 μg/cm^2 when using hyperspectral imagery. Modelling simulations conducted with infinite reflectance models based on Hapke, Lillistaeter and Yamada and Fujimura, and canopy reflectance models SAILH and FLIGHT were linked to PROSPECT-5 to simulate the effects of varying chlorophyll content, leaf structure, canopy LAI and soil reflectance on the retrieval of carotenoid content at the vine-level using the R_{515}/R_{570} index. Simulation results demonstrated that higher accuracy for C_{x+c} estimation is obtained when the retrieval is conducted simultaneously with an index sensitive to C_{a+b} content, such as TCARI/OSAVI. Modelling results suggested that C_{x+c} can be retrieved with r^2=0.93 and RMSE=0.73 μg/cm^2 when both R_{515}/R_{570} and TCARI/OSAVI are used in the scaling up relationships developed through infinite reflectance and canopy simulation models.

Experimental results conducted at the leaf and canopy level through three years of multispectral and hyperspectral airborne flights using an unmanned aerial vehicle confirmed the modelling results obtained with synthetic spectra simulations under different scenarios. Results demonstrated the sensitivity of the R_{515}/R_{570} index to C_{x+c} content at the leaf level (r^2=0.84) and at the airborne level, yielding errors below 1.3 μg/cm^2 for the two years investigated with hyperspectral imagery. Scaling up methods which used simpler approaches, such as the infinite reflectance formulation by Yamada and Fujimura yielded better results than more complex canopy models such as SAILH and FLIGHT. Simpler approaches ($R_{\infty 2}$ yielded RMSE<0.95 μg/cm^2 in the modelling conducted) were comparable to more complex canopy reflectance approximations. Therefore, dark dense approximations performed comparable to the canopy simulations because very high spatial resolution was used to extract pure vine reflectance from the hyperspectral imagery, removing mixed pixels and soil effects. Under such conditions, C_{x+c} estimates using R_{515}/R_{570} (sensitive to C_{x+c}) and TCARI/OSAVI (sensitive to C_{a+b}) yielded RMSE values for $R_{\infty 2}$ below 0.95 $\mu g/cm^2$, while FLIGHT and SAILH obtained errors of 1.3 $\mu g/cm^2$ for the two years investigated with the hyperspectral imagery. Results obtained for the 2010 and 2011 years with hyperspectral imagery yielded lower RMSE values than with estimates conducted with the multispectral imagery (year 2009).

These results conducted for three years demonstrate that maps of the spatial variability of carotenoid content in vineyards can be obtained with errors below 1 $\mu g/cm^2$ using a micro-hyperspectral imager on board an unmanned aerial vehicle. The very high spatial resolution obtained (40 cm pixel size) along with rich spectral information of 6.4 nm FWHM at 1.85 nm/pixel sampling enabled the generation of C_{x+c} maps using R_{515}/R_{570} and TCARI/OSAVI indices for their application in precision agriculture.

Acknowledgements

Financial support from the Spanish Ministry of Science and Education (MEC) for the project AGL2009-13105 and FEDER funding are gratefully acknowledged. Technical support from Headwall Photonics, UAV Navigation, Tetracam, UAV Services and

Systems, and ELIMCO for the accommodation of airborne requirements, camera support and UAV platform developments is also acknowledged. D. Notario, A. Vera, A. Hornero, and R. Romero are acknowledged for technical support during field and airborne campaigns. The scientific and editorial comments of V. Gonzalez-Dugo are appreciated.

References

Berni, J. A. J., Zarco-Tejada, P. J., Sepulcre-Cantó, G., Fereres, E., Villalobos, F. J. (2009b). Mapping canopy conductance and CWSI in olive orchards using high resolution thermal remote sensing imagery. Remote Sensing of Environment, 113, 2380-2388.

Berni, J.A.J., Zarco-Tejada, P.J., Suarez, L., Fereres, E. (2009). Thermal and Narrow-band Multispectral Remote Sensing for Vegetation Monitoring from an Unmanned Aerial Vehicle. IEEE Transactions on Geoscience and Remote Sensing, 47, (3), 722-738.

Blackburn, G. A. (1998). Quantifying chlorophylls and carotenoids at leaf and canopy scales: An evaluation of some hyperspectral approaches. Remote Sensing of the Environment, 66, 273-285.

Carter, G. A., & Spiering, B. A. (2002). Optical properties of intact leaves for estimating chlorophyll concentration. Journal of Environmental Quality, 31(5), 1424-1432.

Chappelle, E. W. Kim, M. S. & McMurtrey J. E. I. (1992). Ratio analysis of reflectance spectra (RARS): an algorithm for the remote estimation of the concentrations of chlorophyll a, chlorophyll b, and carotenoids in soybean leaves. Remote Sensing of Environment, 39, 239-247.

Demmig-Adams, B., & Adams, W. W. III (1992). Photoprotection and other responses of plants to high light stress. Annual Review of Plant Physiology and Plant Molecular Biology, 43: 599-626.

Demmig-Adams, B. (1998). Survey of thermal energy dissipation and pigment composition in sun and shade leaves. Plant Cell Physiology 39, 474-482.

Feret, J. B., François, C., Asner, G. P., Gitelson, A. A., Martin, R., & Bidel, L. P. R. (2008). PROSPECT-4 and 5: Advances in the leaf optical properties model separating photosynthetic pigments. Remote Sensing of Environment, 112, 3030-3043.

Feret, J. B., François, C., Gitelson, A., Asner, G. P., Barry, K. M., Panigada, C., Richardson A. D., & Jacquemoud, S. (2011). Optimizing spectral indices and chemometric analysis of leaf chemical properties using radiative transfer modeling. Remote Sensing of Environment, 115 (10), 2742-2750.

Frank, H. A., & Cogdell, R. J. (1996) Carotenoids in photosynthesis. Photochemistry. Photobiology. 63, 257-264.

Gamon, J. A., Peñuelas, J., & Field, C. B. (1992). A narrow-waveband spectral index that tracks diurnal changes in photosynthetic efficiency. Remote Sensing of Environment, 41, 35 – 44.

Garrity S. R., Eitel, J. U. H., & Vierling, L. A. (2011) Disentangling the relationships between plant pigments and the photochemical reflectance index reveals a new approach for remote estimation of carotenoid content. Remote Sensing of Environment, 115, 628-635.

Gitelson, A. A., Zur, Y., Chivkunova, O. B., & Merzlyak, M. N. (2002). Assessing carotenoid content in plant leaves with reflectance spectroscopy. Journal of Photochemistry and Photobiology B-Biology, 75, 272-281.

Gitelson, A. A., Keydan, G. P., & Merzlyak, M. N. (2006). Three-band model for noninvasive estimation of chlorophyll, carotenoids, and anthocyanin content in higher plant leaves. Geophysical Research Letters, 33, L11402.

Gitelson, A. A., Gritz, Y., & Merzlyak, M. N. (2003). Relationships between leaf chlorophyll content and spectral reflectance and algorithms for nondestructive chlorophyll assessment in higher plants. Journal of Plant Physiology, 160(3), 271 – 282.

González-Dugo, V., Zarco-Tejada, P.J., Berni, J.A., Suarez, L., Goldhamer, D., Fereres, E. (2012), Almond tree canopy temperature reveals intra-crown variability that is water stress-dependent, Agricultural and Forest Meteorology, 154-155, 156-165.

Gueymard, C.A. (1995). SMARTS, A Simple Model of the Atmospheric Radiative Transfer of Sunshine: Algorithms and Performance Assessment. Technical Report No. FSECPF- 270-95. Cocoa, FL: Florida Solar Energy Center.

Gueymard, C. A. (2001). Parameterized Transmittance Model for Direct Beam and Circumsolar Spectral Irradiance. Solar Energy, 71,. 325-346.

Guillén-Climent, M.L., Zarco-Tejada, P.J., Villalobos, F.J., Mapping radiation interception in vineyards using 3D simulation and high resolution airborne imagery, Precision Agriculture (submitted).

Guillén-Climent, M.L., Zarco-Tejada, P.J., Berni, J.A.J., North, P.R.J., Villalobos, F.J., Mapping radiation interception in row-structured orchards using 3D simulation and high resolution airborne imagery acquired from an UAV, Precision Agriculture (in press).

Haboudane, D., Miller, J. R., Pattey, E., Zarco-Tejada, P. J., & Strachan, I. (2004). Hyperspectral vegetation indices and novel algorithms for predicting green LAI of crop canopies: Modeling and validation in the context of precision agriculture. Remote Sensing of Environment, 90(3), 337 – 352.

Haboudane, D., Miller, J. R., Tremblay, N., Zarco-Tejada, P. J., & Dextraze, L. (2002). Integration of hyperspectral vegetation indices for prediction of crop chlorophyll content for application to precision agriculture. Remote Sensing of Environment, 81(2 – 3), 416 – 426.

Hapke, B. (1993). Theory of Reflectance and Emittance Spectroscopy. Cambridge, U.K Univ. Press.

Hernández-Clemente, R., Navarro-Cerrillo, R., Suárez, L., Morales, F., Zarco-Tejada, P.J. (2011). Assessing structural effects on PRI for stress detection in conifer forests, Remote Sensing of Environment, 115(9), 2360-2375.

Hernández-Clemente, R., Navarro-Cerrillo, R. M., Zarco-Tejada, P. J., Carotenoid content estimation in an heterogeneous conifer forest using narrow-band indices and PROSPECT + DART simulations. Remote Sensing of Environment (submitted).

Jaquemoud, S. and Baret, F., (1990). Prospect: A model of leaf optical properties spectra. Remote Sensing of Environment, 34, 75-91.

Jacquemoud, S., Ustin, S. L., Verdebout, J., Schmuck, G., Andreoli, G., & Hosgood, B. (1996). Estimating leaf biochemistry using the PROSPECT leaf optical properties model. Remote Sensing of Environment, 56, 194 - 202.

Kuusk, A. (1985). The hotspot effect of a uniform vegetation cover. Soviet Journal of Remote Sensing, 3: 646-658.

le Maire, G., Franc¸ois, C., & Dufrene, E. (2004). Towards universal broad leaf chlorophyll indices using PROSPECT simulated database and hyperspectral reflectance measurements. Remote Sensing of Environment, 89, 1 – 28.

Lillestaeter, O. (1982). Spectral reflectance of partly transmitting leaves: Laboratory measurements and mathematical modeling, Remote Sensing of Environmet, 12, 247-254.

Martin, P., Zarco-Tejada, P., González, M. R. & Berjon, A. (2007). Using Hyperspectral Remote Sensing to mapgrape quality in 'Tempranillo' Vineyards affected by Iron deficiency Chlorosis, Vitis, 46 (1).

Meggio F., Zarco-Tejada, P. J., Núñez L. C., Sepulcre-Cantó G., Gonzalez M. R. & Martin, P. (2010). Grape quality assessment in vineyards affected by iron deficiency chlorosis using narrow-band physiological remote sensing indices. Remote Sensing of Environment, 114, 1968-1986.

Merzlyak, M. N., Gitelson, A. A., Chivkunova, O. B., & Rakitin, V. Y. (1999). Non destructive optical detection of leaf senescence and fruit ripening. Physiologia Plantarum, 106, 135- 141.

Miller, J. R., Steven, M. D. & Demetriades-Shah, T. H. (1992). Reflection of layered bean leaves over different soil backgrounds: measured and simulated spectra. International Journal of Remote Sensing, 13, 3273–3286.

North. P.R.J. (1996). Three-Dimensional Forest Light Interaction Model Using a Monte Carlo Method. IEEE Transaction on Geoscience and Remote Sensing, 34, (4), 946-956.

Peñuelas, J., Filella, I., Lloret, P., Muñoz, F., & Vilajeliu, M. (1995). Reflectance assessment of mite effects on apple trees. International Journal of Remote Sensing, 16–14, 2727–2733.

Riaño, D., M. A. Patricio, P. J. Zarco-Tejada, C. Rueda, L & Usero, S. L. Ustin (2005). Estimation of equivalent water thickness using radial basis function neural networks. International Conference on Remote Sensing and Geoinformation Processing in the Assessment and Monitoring of Land Degradation and Desertification (RGLDD), Trier (Germany), 7-9/09/2005.

Ritz T., Damjanovic, A., Schulten, K., Zhang, J. P. & Koyama, Y. (2000). Understanding efficient light-harvesting through carotenoids with novel theoretical and experimental techniques. Photosynth Research, 66, 125-144.

Rondeaux, G., Steven, M., & Baret, F. (1996). Optimization of soil-adjusted vegetation indices. Remote Sensing of Environment, 55, 95 - 107.

Sims, D. A., & Gamon, J. A. (2002). Relationships between leaf pigment content and spectral reflectance across a wide range of species, leaf structures and developmental stages. Remote Sensing of Environment, 81, 337 – 354.

Suárez, L., Zarco-Tejada, P. J., Sepulcre-Cantó, G., Pérez-Priego, O., Miller, J. R., Jiménez-Muñoz, J. C., & Sobrino, J. (2008). Assessing canopy PRI for water stress detection with diurnal airborne imagery. Remote Sensing of Environment, 112, 560-575.

Suárez, L., Zarco-Tejada, P. J., González-Dugo, V., Berni, J. A. J., Sagardoy, R., Morales, F. & Fereres, E. (2010). Detecting water stress effects on fruit quality in orchards with time-series PRI airborne imagery. Remote Sensing of Environment, 114, 286-298.

Thayer, S. S., & Björkman, O. (1990). Leaf xanthophyll content and composition in sun and shade determined by HPLC. Photosynthesis Research, 23, 331–343.

Verhoef, W. (1984). Light scattering by leaf layers with application to canopy reflectance modeling: the SAIL model. Remote Sens. Environ., vol. 16, pp. 125–141.

Wellburn, A. R. (1994). The spectral determination of chlorophylls a and b, as well as total carotenoids using various solvents with spectrophotometers of different resolutions. Journal of Plant Physiology, 144, 307 – 313.

Yamada, N. & Fujimura, S. (1991), Nondestructive measurement of chlorophyll pigment content in plant leaves from three-color reflectance and transmittance. Applied Optics,30, 3964-3973.

Young, A. & Britton, G. (1990). Carotenoids and stress. In Alscher, R. G., Cumming, J. R. (Ed.), Stress responses in plants: adaptation and acclunation mechanisms (pp. 87-112).

Zarco-Tejada, P. J., Miller, J. R., Mohammed, G. H., Noland, T. L., & Sampson, P. H. (2001). Scaling-up and model inversion methods with narrow-band optical indices for chlorophyll content estimation in closed forest canopies with hyperspectral data. IEEE Transactions on Geoscience and Remote Sensing, 39(7), 1491 -1507.

Zarco-Tejada, P. J., Miller, J. R., Morales, A., Berjón, A., & Agüera, J. (2004). Hyperspectral indices and model simulation for chlorophyll estimation in open-canopy tree crops. Remote Sensing of Environment, 90(4), 463- 476.

Zarco-Tejada, P.J., Berjón, A., López-Lozano, R., Miller, J.R., Martín, P., Cachorro, V., González, M.R., Frutos, A. (2005), Assessing Vineyard Condition with Hyperspectral Indices: Leaf and Canopy Reflectance Simulation in a Row-Structured Discontinuous Canopy. Remote Sensing of Environment, 99, 271-287.

Zarco-Tejada, P.J., Berni, J.A.J., Suárez, L. & Fereres, E. (2008). A new era in remote sensing of crops with unmanned robots. SPIE Newsroon, doi:10.1117/2.1200812.1438.

Zarco-Tejada, P.J., Berni, J.A.J., Suárez, L., Sepulcre-Cantó, G., Morales, F., Miller, J.R. (2009), Imaging Chlorophyll Fluorescence from an Airborne Narrow-Band Multispectral Camera for Vegetation Stress Detection, Remote Sensing of Environment, 113, 1262-1275.

Zarco-Tejada, P. J., González-Dugo, V., & Berni, J. A. J., (2012). Fluorescence, temperature and narrow-band indices acquired from a UAV platform for water stress detection using a micro-hyperspectral imager and a thermal camera. Remote Sensing of Environment, 117, 322-337.

Table 1. Measured parameters for the vine study sites used in this study, showing the variability in row orientation, width, height and LAI.

Plot	Row orientation (º)	Planting grid (m)	Width (m)	Height (m)	LAI
1	96.05	3 x 1.5	0.6	1.3	1.1
2	93.06	3 x 1.5	0.55	1.4	0.8
3	20.07	3 x 1.5	0.2	0.8	0.3
4	20.07	3 x 1.5	0.4	0.8	0.5
5	103.1	3 x 1.5	0.5	1.15	0.96
6	103.1	3 x 1.5	0.6	1.05	1.15
7	93.06	3 x 1.5	0.7	1.32	1.26
8	75.2	3 x 1.5	0.9	1.5	1.4
9	1.02	3 x 1.5	0.8	1.4	1.4
10	1.02	3 x 1.5	0.6	1.2	0.8
11	93.06	3 x 1.5	0.41	0.7	0.4
12	93.06	3 x 1.5	0.7	1.5	1.2
13	47.5	3 x 1.5	0.6	1.2	0.75
14	47.5	3 x 1.5	0.55	0.9	0.6
15	47.5	3 x 1.5	0.8	1.1	0.8
16	28.5	3 x 1.5	0.9	1.3	1.48
17	28.5	3 x 1.5	1.1	1.7	1.3
18	49.5	3 x 1.5	0.8	1.45	1.07
19	49.5	3 x 1.5	0.6	1.45	1.25
20	61.42	3 x 1.5	0.75	1.4	1.56
21	61.42	3 x 1.5	0.85	1.35	1.37

Table 2. Nominal values and range of parameters used for leaf and canopy simulation with PROSPECT-5, SAILH and FLIGHT for pure vine reflectance simulation.

PROSPECT	*Nominal values and range*
Chlorophyll a+b C_{a+b} *($\mu g\ cm^{-2}$)*	30-80
Carotenoid content C_{x+c} *($\mu g\ cm^{-2}$)*	4-14
Leaf water content, C_w *(cm)*	0.025
Leaf dry matter content, C_m *($g\ cm^{-2}$)*	0.03
Leaf internal structure parameter, *N*	1.6-1.8
SAILH	
Leaf reflectance and transmittance	PROSPECT-5 simulations
Soil reflectance	Random (0-1)
Leaf area index	1-3
Lead angle distribution function	ε = 0.95; θn = 45º (plagiophile)
Viewing geometry (θs θv ϕ)	Calculated for each image & site
Hotspot parameter	0.083
FLIGHT	
Hemispherical reflectance and transmittance of green leaves	PROSPECT-5 simulations
Hemispherical reflectance and transmittance of senescent leaves	Not used
Leaf equivalent radius	0.083 m
Leaf area index (LAI)	1-3
Fractional cover	Estimated from Table 1
Leaf Angle Distribution Function (LADF)	Plagiophile
Fraction of green leaves	1
Fraction of senescent leaves	0
Fraction of bark	0
Number of stands and position coordinates	Not used
Crown shape	Elliptical
Crown height and radius	From Table 1 (m)
Trunk height and radius	Field measured
Viewing geometry angles	Calculated for each image & site
Soil reflectance	From image
Soil roughness	0
Aerosol Optical Depth (AOD)	Measured at the time of flights

Table 3. Simulation study conducted with PROSPECT-5 and different canopy approximations through infinite reflectance R_∞ formulations and SAILH.

	PROSPECT-5 + $R_{\infty 1}$		**PROSPECT-5 + $R_{\infty 2}$**		**PROSPECT-5 + $R_{\infty 3}$**		**PROSPECT-5 + SAILH**	
	R^2	**RMSE ($\mu g/cm^2$)**	**R^2**	**RMSE ($\mu g/cm^2$)**	**R^2**	**RMSE ($\mu g/cm^2$)**	**R^2**	**RMSE ($\mu g/cm^2$)**
CASE 1 **C_{x+c}*, C_{a+b}, N, LAI, ρ_{soil}**	0.99	0.08	0.99	0.06	0.99	0.07	0.99	0.08
CASE 2 **C_{x+c}*, C_{a+b}, N*, LAI*, ρ_{soil}***	0.99	0.15	0.98	0.33	0.99	0.07	0.98	0.29
CASE 3 **C_{x+c}*, C_{a+b}*, N, LAI, ρ_{soil}**	0.51	1.97	0.74	1.46	0.61	1.78	0.5	1.99
CASE 4 **C_{x+c}*, C_{a+b}*, N*, LAI*, ρ_{soil}***	0.54	1.97	0.72	1.56	0.62	1.83	0.51	1.99
CASE 5 **C_{x+c}*, C_{a+b}*, N*, LAI*, ρ_{soil}***	0.96	0.58	0.73	1.49	0.97	0.46	0.93	0.73

Cases 1 to 4 are models $C_{x+c}=f(R_{515}/R_{570})$;
Case 5 is a model considering chlorophyll content through TCARI/OSAVI: $C_{x+c}=f(R_{515}/R_{570}; TCARI/OSAVI)$.

Table 4. Coefficients of determination and RMSE obtained for three years of airborne imagery for C_{x+c} estimation (C_{x+c} = f(R_{515}/R_{570}; TCARI/OSAVI)) through scaling up. Models used were PROSPECT-5 linked with three infinite reflectance formulations ($R_{\infty 1}$; $R_{\infty 2}$; $R_{\infty 3}$), SAIL and FLIGHT.

		PROSPECT-5 + $R_{\infty 1}$		PROSPECT-5 + $R_{\infty 2}$		PROSPECT-5 + $R_{\infty 3}$		PROSPECT-5 + SAILH		PROSPECT-5 + FLIGHT	
		R^2	**RMSE (µg/cm^2)**	**R^2**	**RMSE (µg/cm^2)**	**R^2**	**RMSE (µg/cm^2)**	**R^2**	**RMSE (µg/cm^2)**	**R^2**	**RMSE (µg/cm^2)**
C_{x+c}=f(R_{515}/R_{570};TCARI/OSAVI)	**2009**	0.28	2.4	0.41	1.6	0.19	4.4	0.2	4.6	0.26	2.91
	2010	0.59	3.4	0.64	0.94	0.56	1.08	0.56	1.28	0.58	1.32
	2011	0.44	3.2	0.44	0.8	0.28	0.93	0.44	1.08	0.55	1.25

Figure 1. Hyperspectral scene (a) obtained with the micro-hyperspectral imager on board the UAV platform at 40 cm resolution, enabling pure vine identification (b). The imagery enabled the separation of pure vine from shaded and sunlit soil reflectance (c), observing the scene components and the pure vine reflectance later used for index calculation (d).

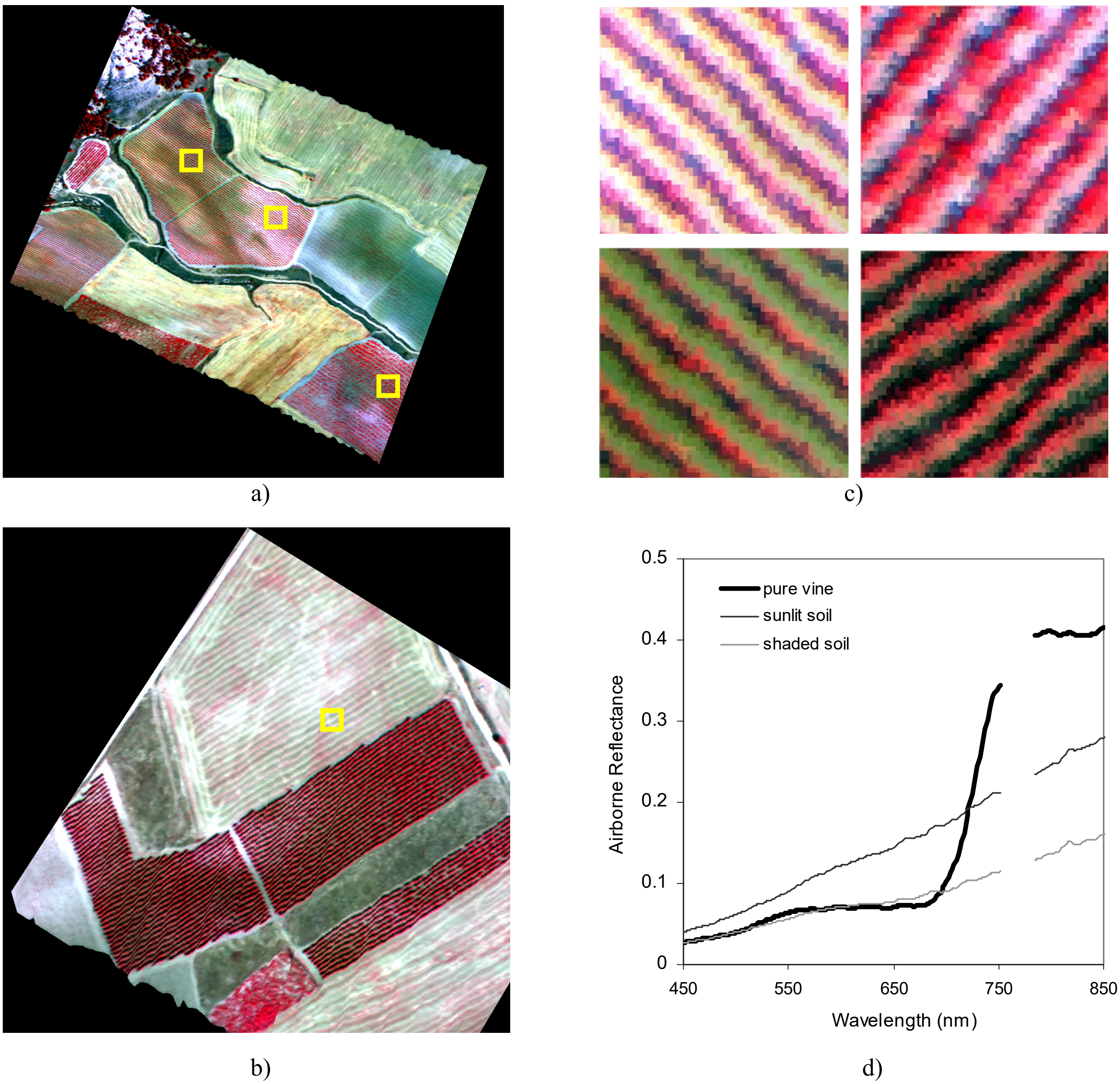

Figure 2. Mean reflectance extracted from the imagery acquired with the micro-hyperspectral imager on board the UAV platform flown over the vineyard sites. Reflectance shown consisted on 260 spectral bands at 6.4 nm FWHM and 40 cm resolution.

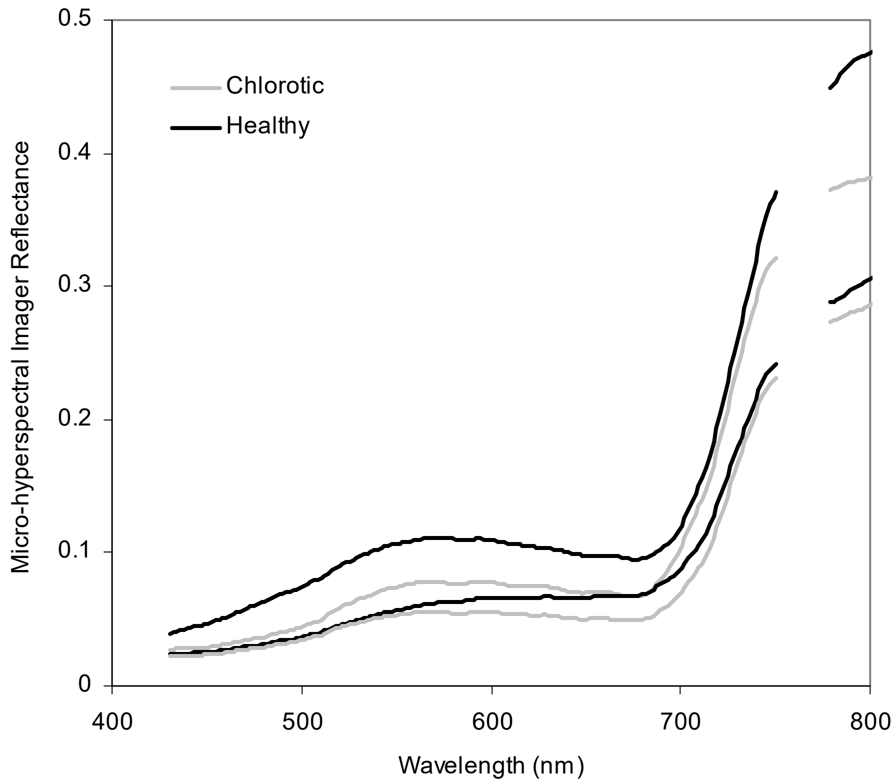

Figure 3. Simulations conducted with PROSPECT-5 in the 400-600 nm region for varying C_{x+c} (4-14 μg/cm^2) (a;b) and chlorophyll C_{a+b} (30-80 μg/cm^2) (c;d) for fixed N=1.6, C_w=0.025 cm, and C_m=0.03 g/cm^2. C_{x+c} and C_{a+b} units are in μg/cm^2.

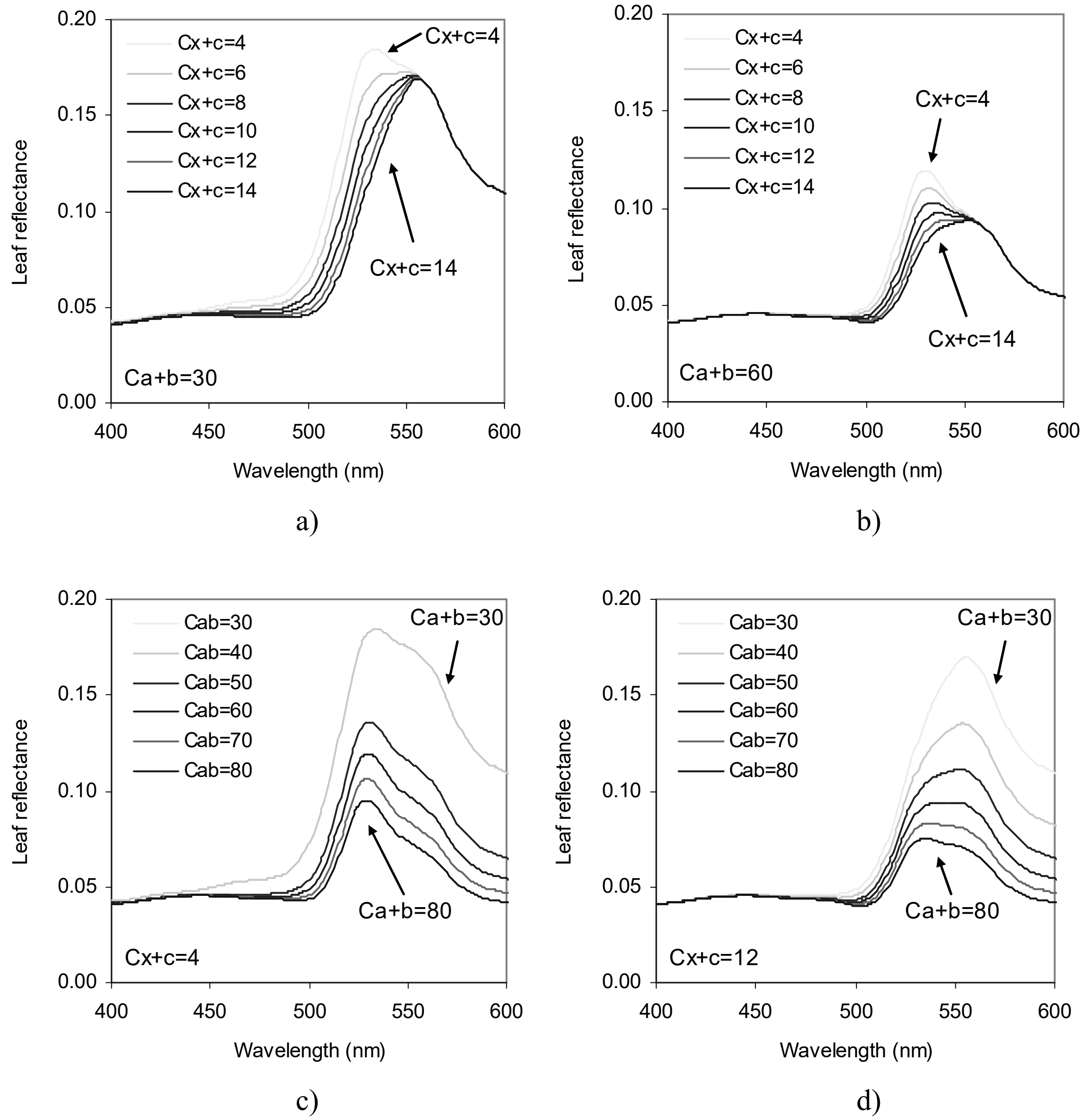

Figure 4. Images acquired by the hyperspectral imager on board the UAV platform over two vineyards with opposite row orientation (a;b), showing the corresponding simulated scene generation with FLIGHT (c;d). The simulated canopy reflectance extracted from the center of the row and aggregated scenes are shown (e;f)

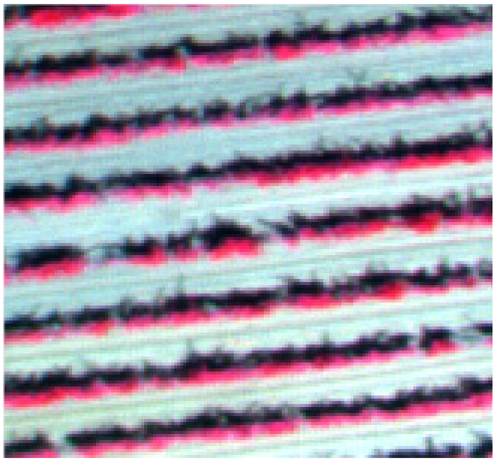

a)

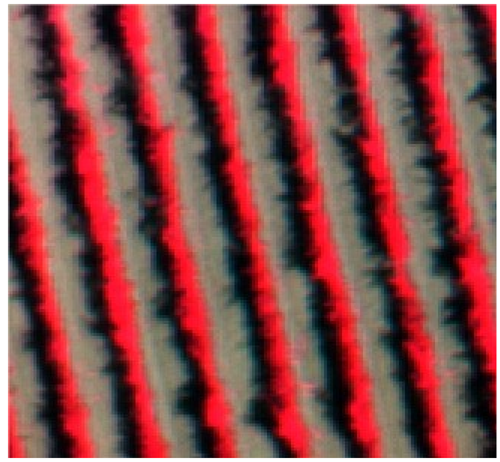

b)

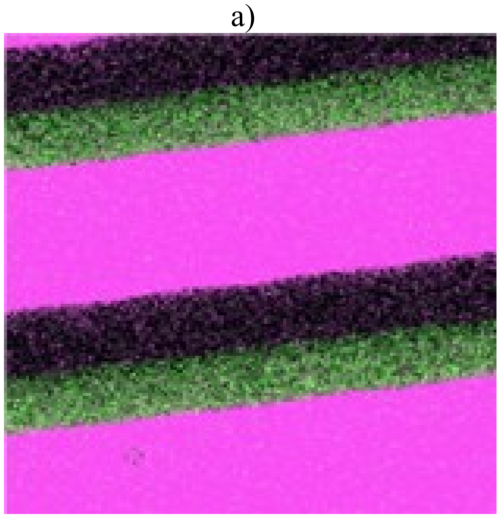

c)

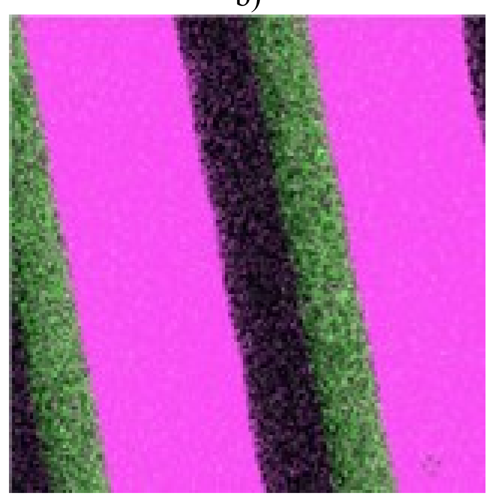

d)

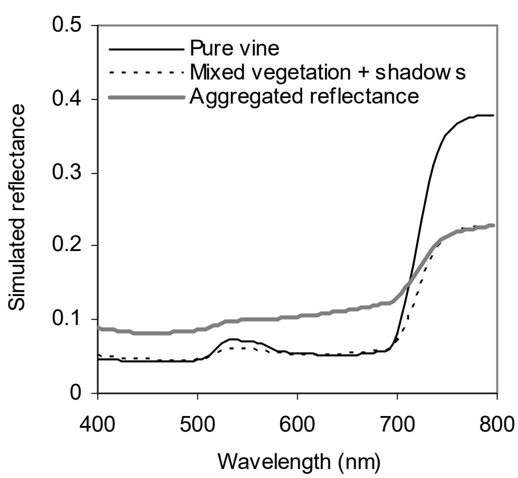

e)

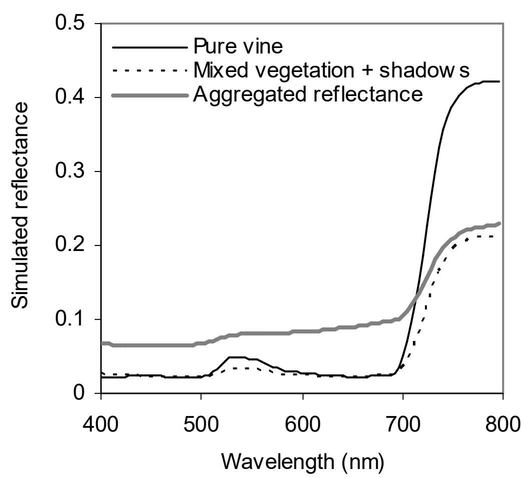

f)

Figure 5. Modelling results conducted with PROSPECT-5 + SAILH for R_{515}/R_{570} and C_{x+c} as a function of C_{a+b} content (a), N parameter (b), LAI (c) and soil reflectance variation (d).

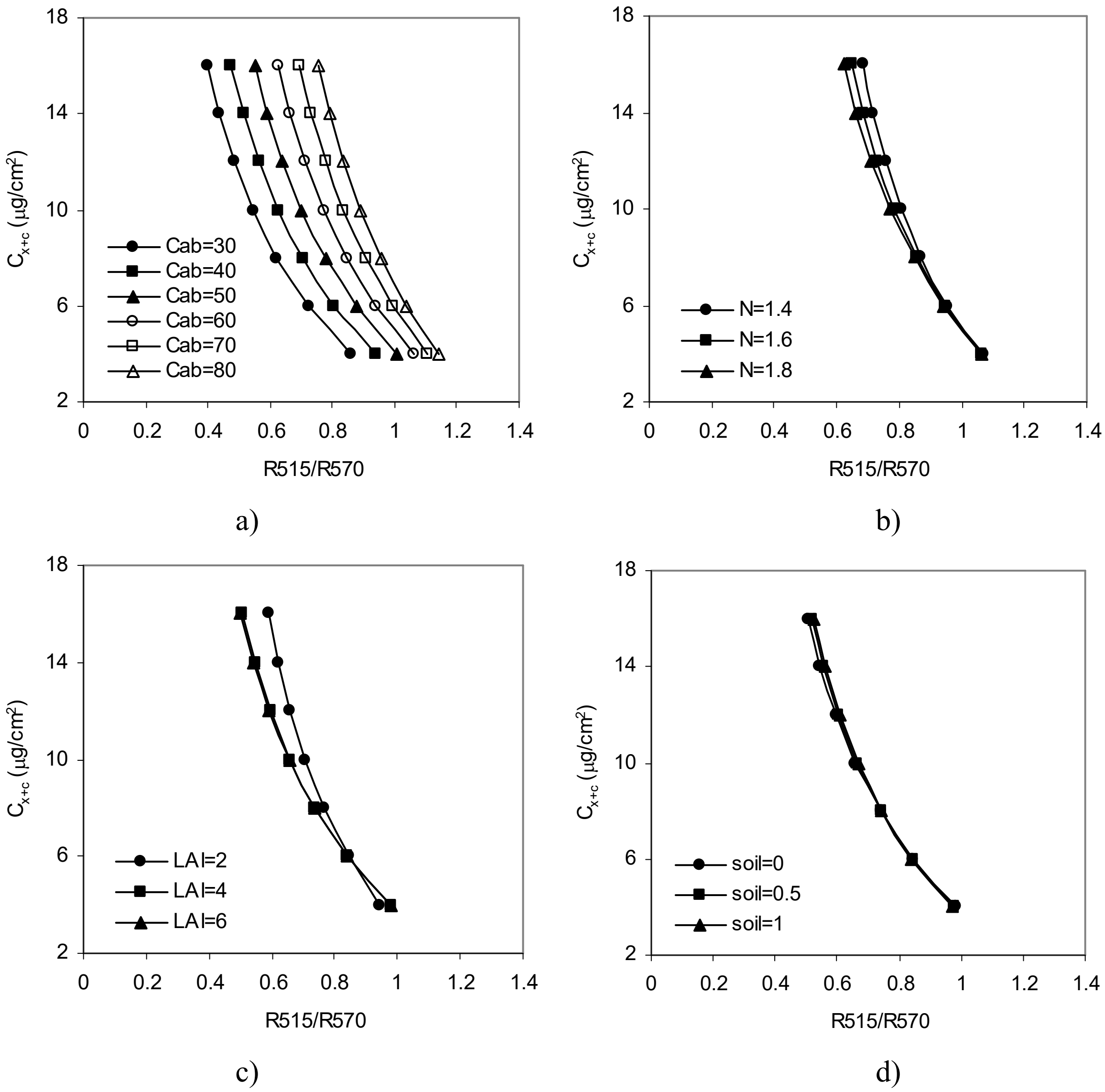

Figure 6. Relationship obtained at the leaf level between the index R_{515}/R_{570} measured with the customized PlantPen instrument and C_{x+c} measured by destructive sampling.

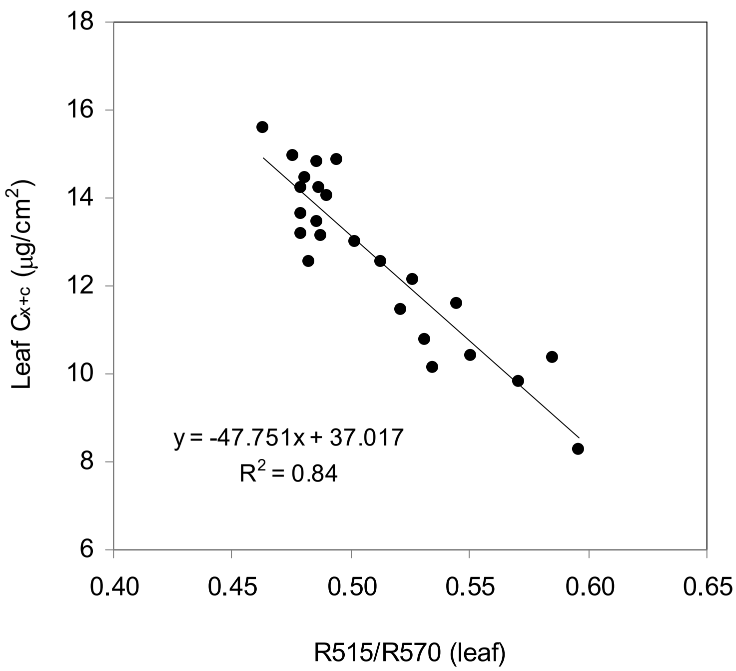

Figure 7. Relationships obtained between the R_{515}/R_{570} index obtained for each vineyard site from the airborne hyperspectral imagery and C_{x+c} measured in the field for the three years under study.

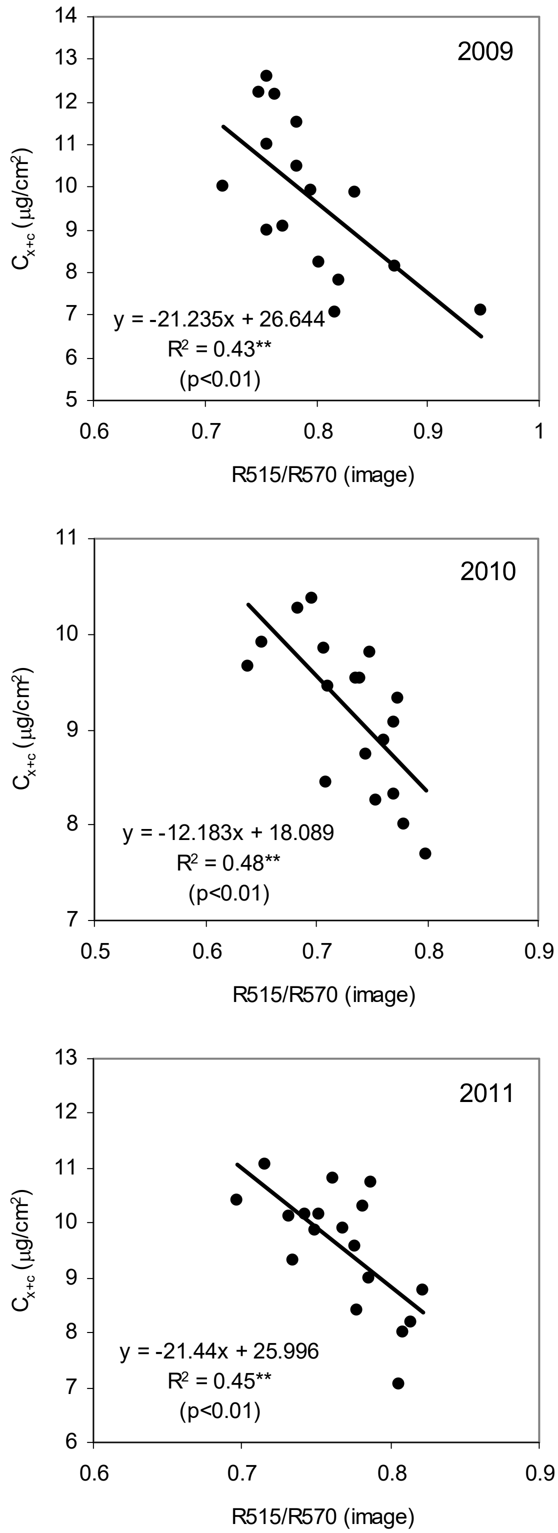

Figure 8. Relationship obtained between the TCARI/OSAVI index obtained for each vineyard site from the airborne hyperspectral imagery and C_{a+b} measured in the field for the year 2010.

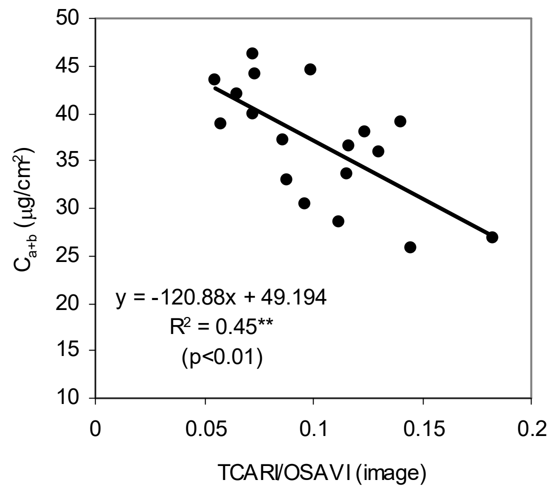

Figure 9. Validation results obtained for the estimation of C_{x+c} from the airborne hyperspectral imagery for the years 2010 and 2011 using R_{515}/R_{570} and TCARI/OSAVI using infinite reflectance formulations (a), SAILH and FLIGHT (b).

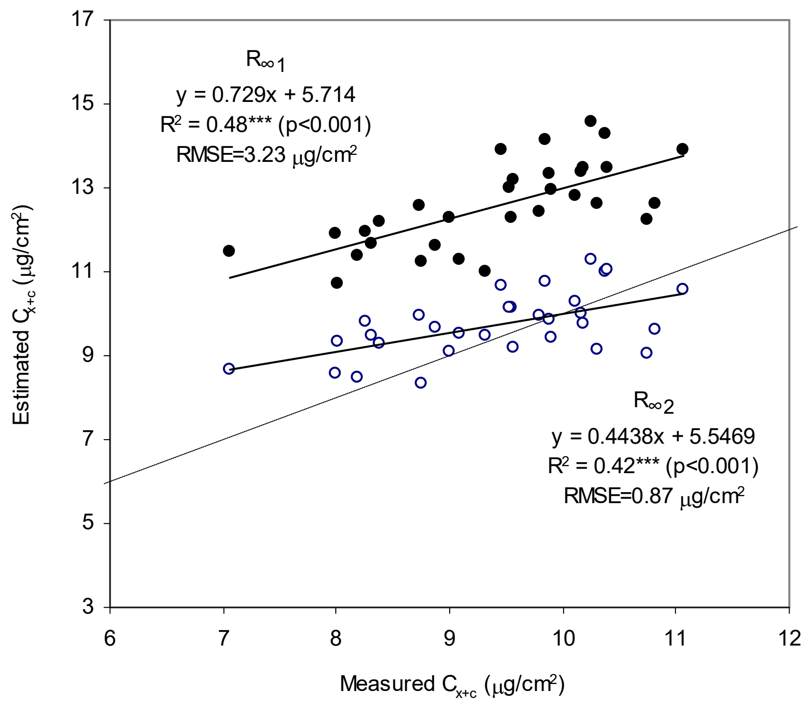

(a)

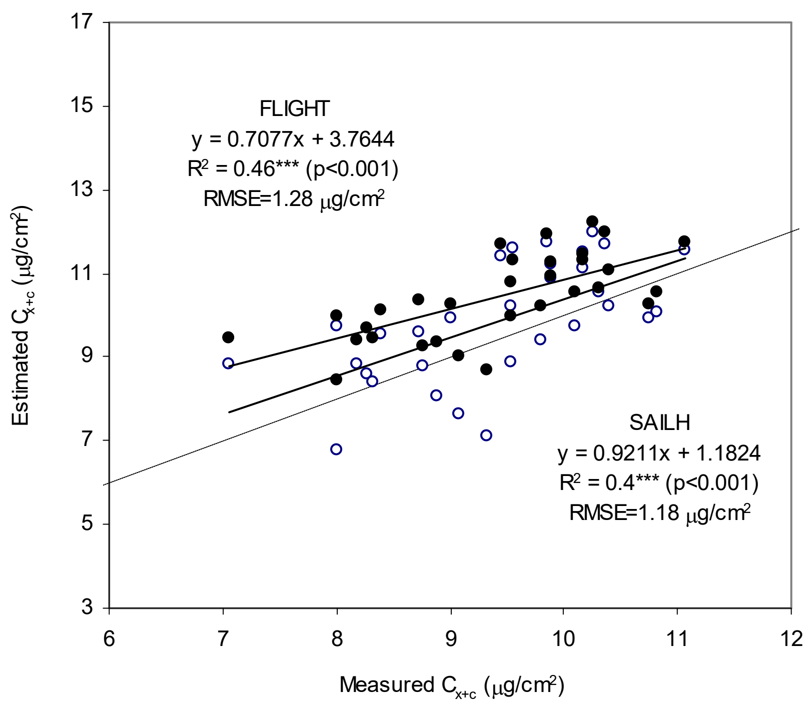

(b)

Figure 10. Mapping results obtained on two sample vineyard fields (a;c) acquired with the hyperspectral imager on board the unmanned aerial vehicle. C_{x+c} content was estimated from indices R_{515}/R_{570} and TCARI/OSAVI using FLIGHT.